Electronic Supplementary Information (ESI)

Enhancement of the catalytic activity of lithium amide towards ammonia decomposition by addition of transition metals

Caitlin A. Brooker-Davis[a], Joshua W. Makepeace[a], Thomas J. Wood[b]*

[a]Haworth Building, University of Birmingham, Birmingham, B15 2TT
[b]ISIS Facility, Rutherford Appleton Laboratory, Harwell, Didcot, OX11 0QX
**Corresponding author: J.W.Makepeace@bham.ac.uk*

Table of contents

Component gas flow during transition metal-only ammonia decomposition experiments

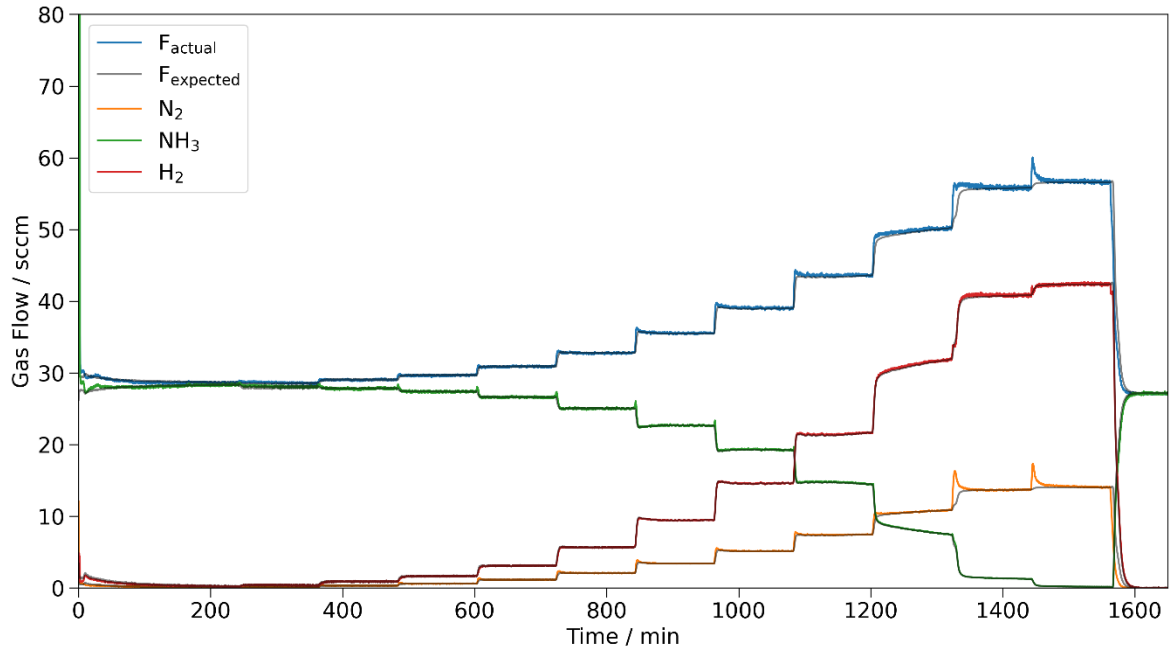

Figure S 1: Total, component, and expected gas flows for the Cr-only (0.5 g) ammonia decomposition experiment.

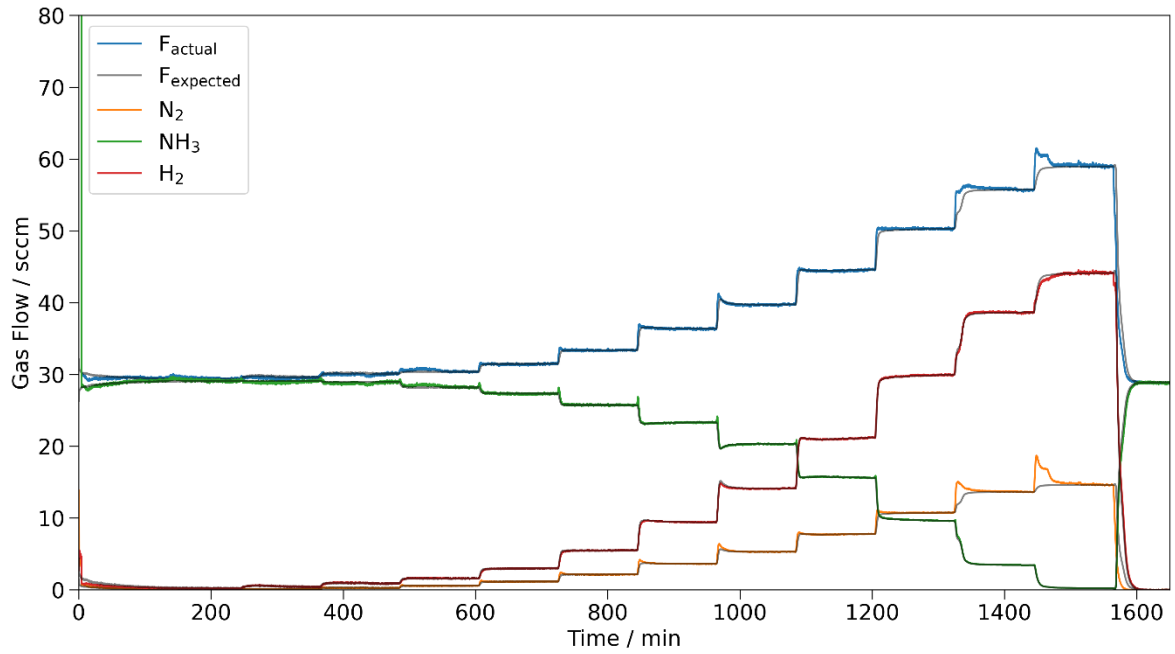

Figure S 2: Total, component, and expected gas flows for the Fe-only (0.5 g) ammonia decomposition experiment.

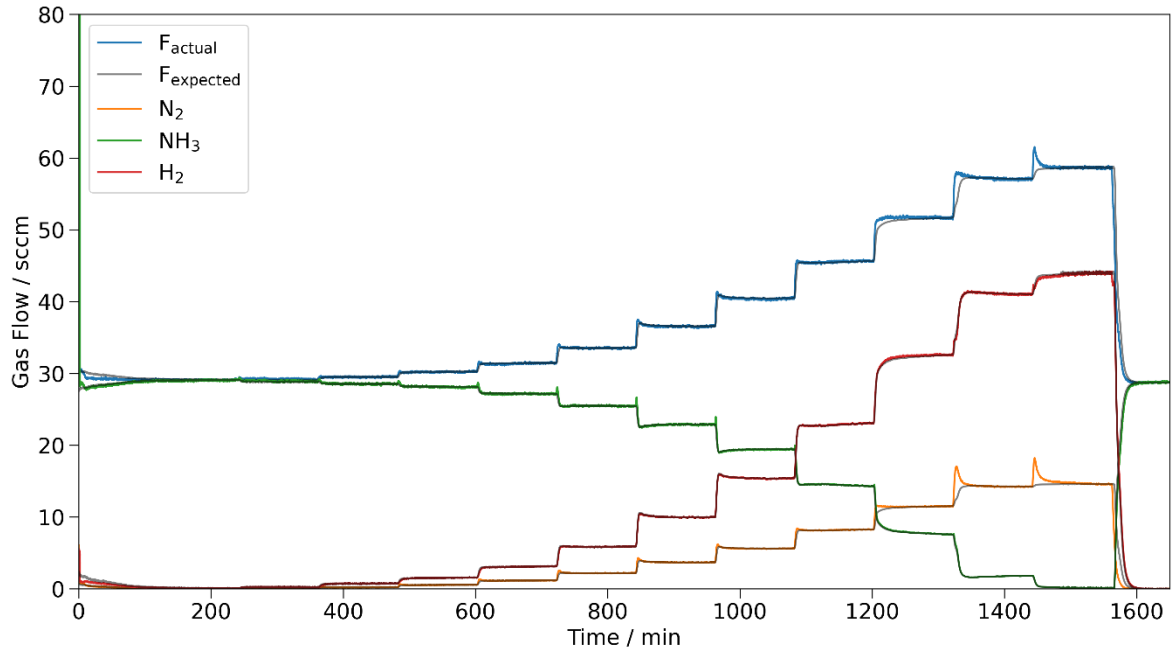

Figure S 3: Total, component, and expected gas flows for the Mn-only (0.5 g) ammonia decomposition experiment.

Component gas flow during $LiNH_2$ ammonia decomposition experiment

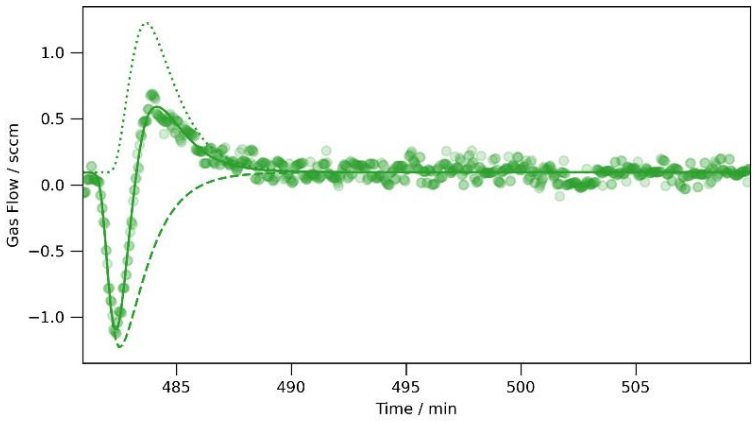

Figure S 4: Double exponential fit to the ammonia gas flow profile of the $LiNH_2$ ammonia decomposition experiment at 480 min (temperature rise to 380°C). The time constant for each exponential decay was 1.15(4) min.

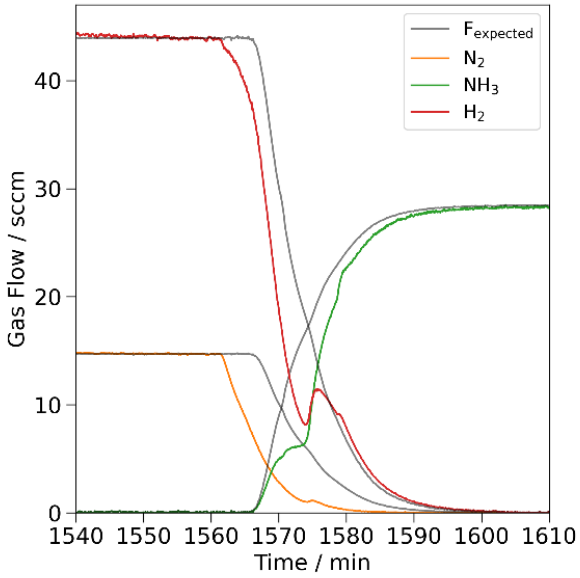

Figure S 5: Measured and expected component gas flows during the cool down period of the $LiNH_2$ ammonia decomposition experiment (1560 min onwards). A less than expected NH_3 flow is related to the absorption of NH_3 by the Li_2NH-rich phase to re-form the $LiNH_2$ starting material.

Exponential fits to the N_2 flow during ammonia decomposition experiments

Blank experiment

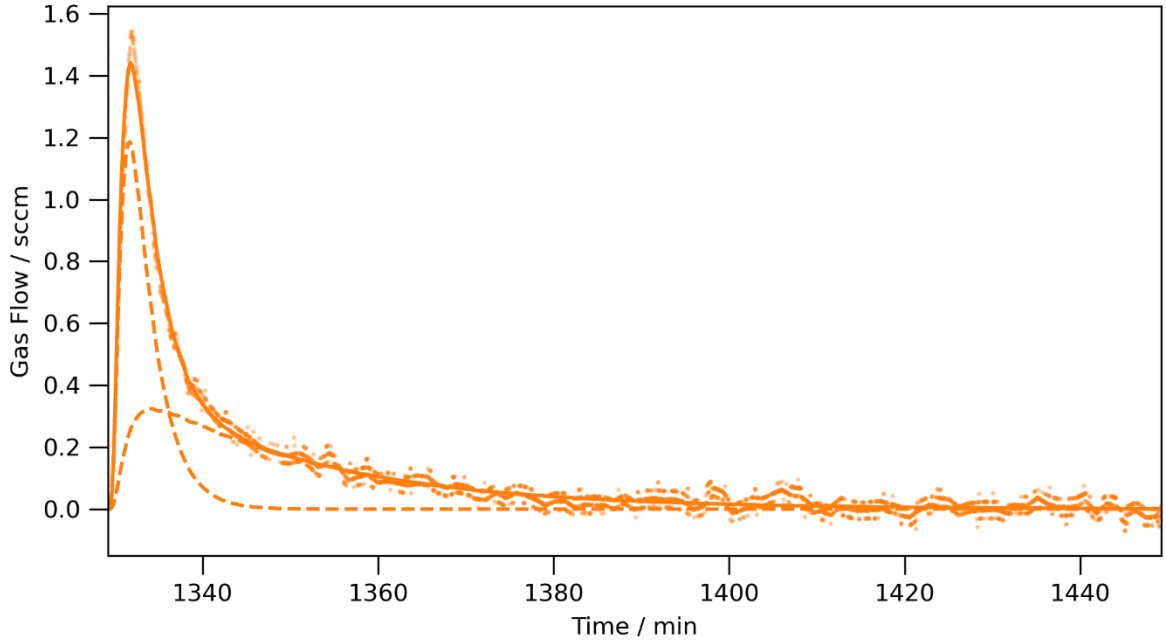

Figure S 6: Double exponential fit to the N_2 release at 500°C for the blank reactor experiment. Dotted and dashed lines correspond with each component exponential curve, while the solid line is the summed fit.

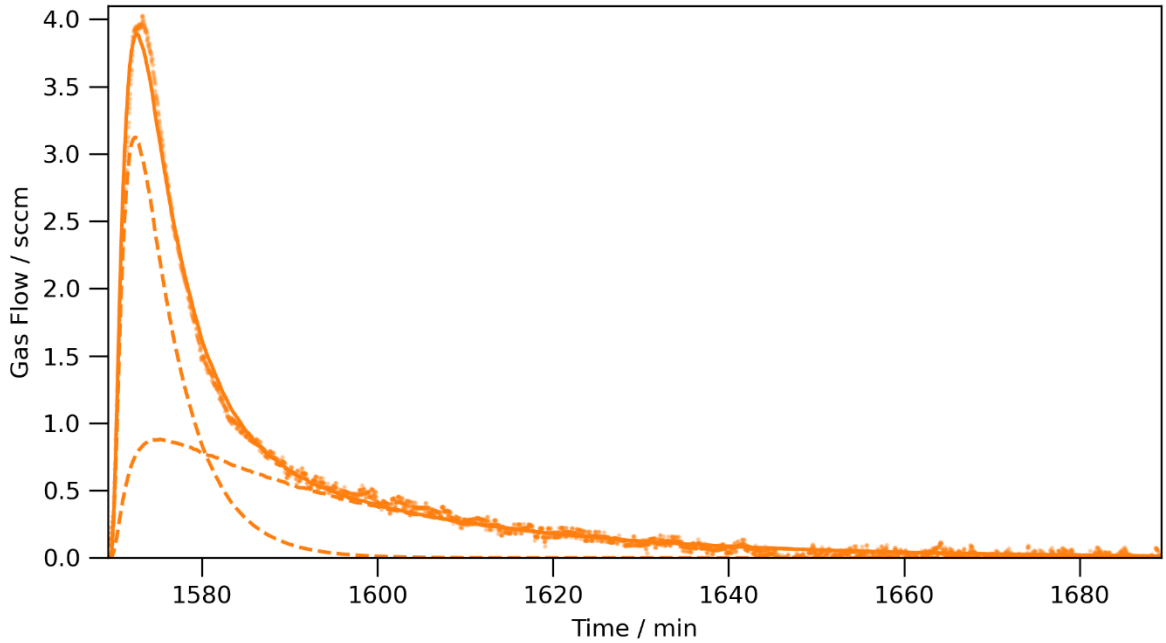

Figure S 7: Double exponential fit to the N_2 release at 540°C for the blank reactor experiment. Dotted and dashed lines correspond with each component exponential curve, while the solid line is the summed fit.

$LiNH_2$ experiment

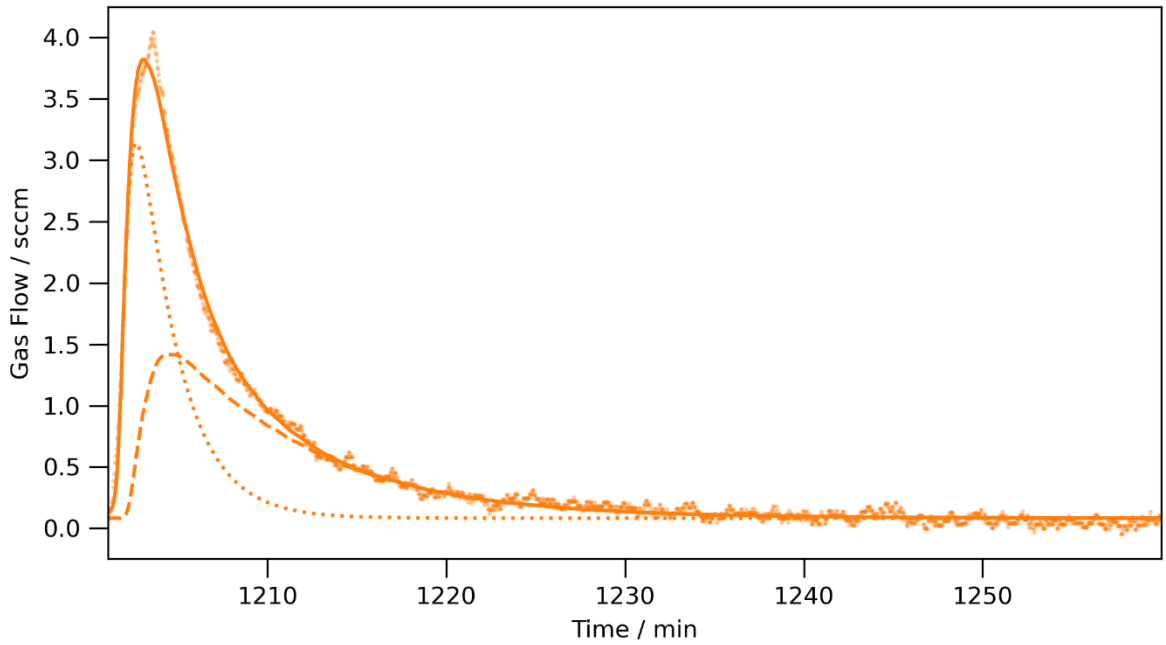

Figure S 8: Double exponential fit to the N_2 release at 500°C for the $LiNH_2$ experiment. Dotted and dashed lines correspond with each component exponential curve, while the solid line is the summed fit.

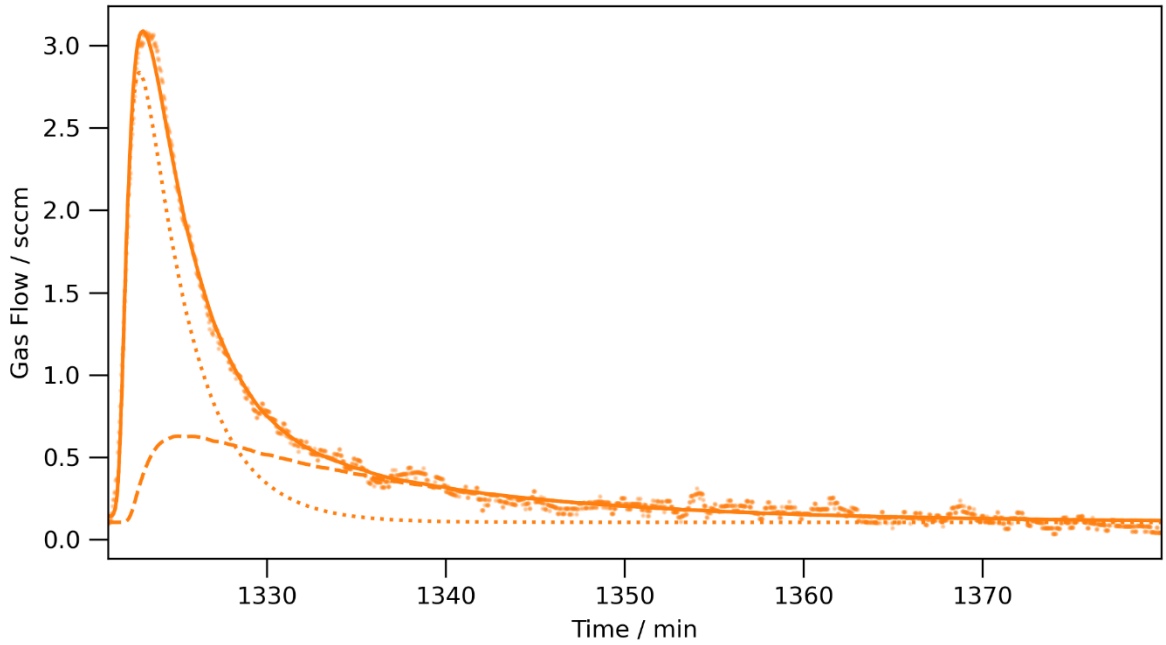

Figure S 9: Double exponential fit to the N_2 release at 520°C for the $LiNH_2$ experiment. Dotted and dashed lines correspond with each component exponential curve, while the solid line is the summed fit.

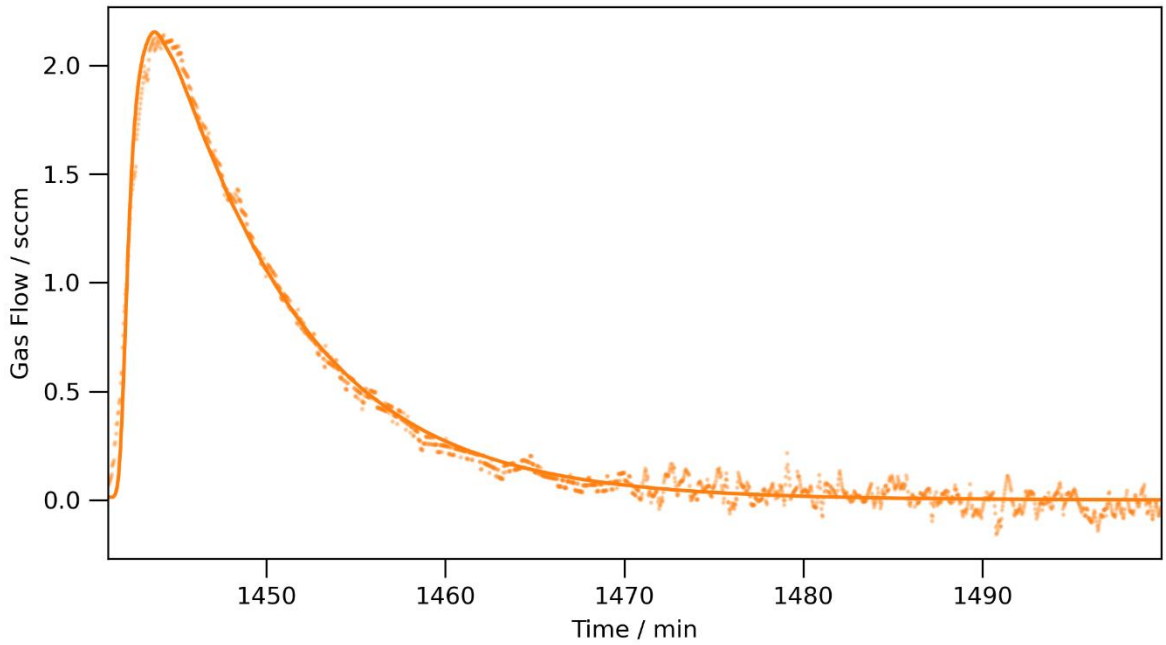

Figure S 10: Single exponential fit to the N_2 release at 540°C for the $LiNH_2$ experiment.

<u>$LiNH_2$-Cr experiment</u>

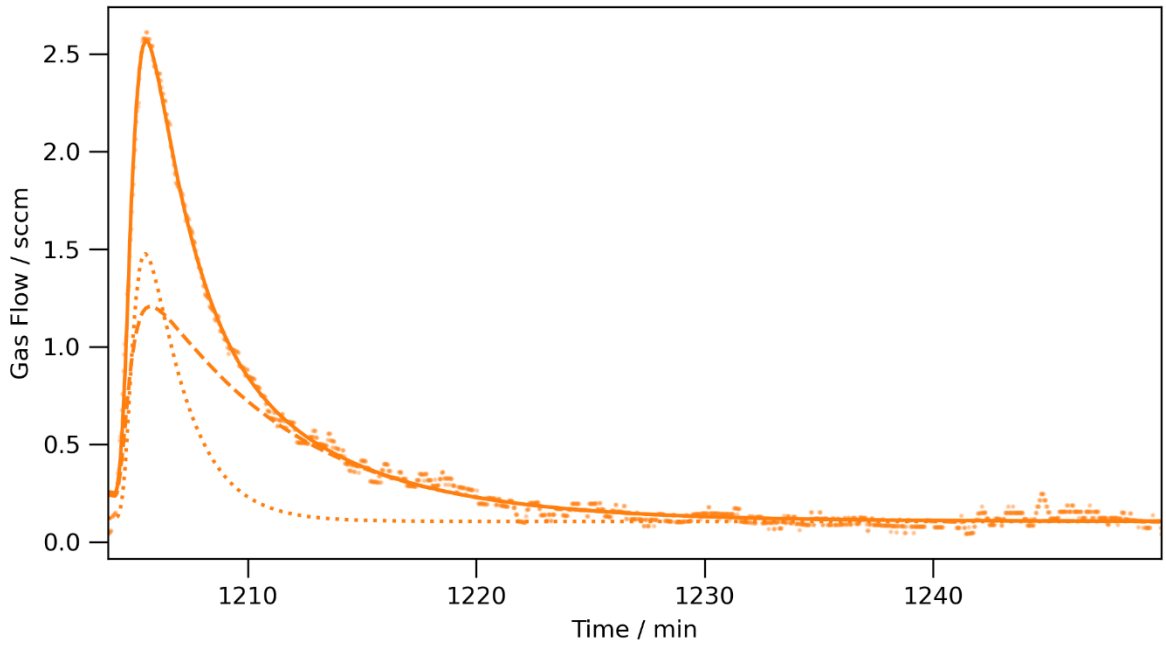

Figure S 11: Double exponential fit to the N_2 release at 500°C for the $LiNH_2$-Cr experiment. Dotted and dashed lines correspond with each component exponential curve, while the solid line is the summed fit.

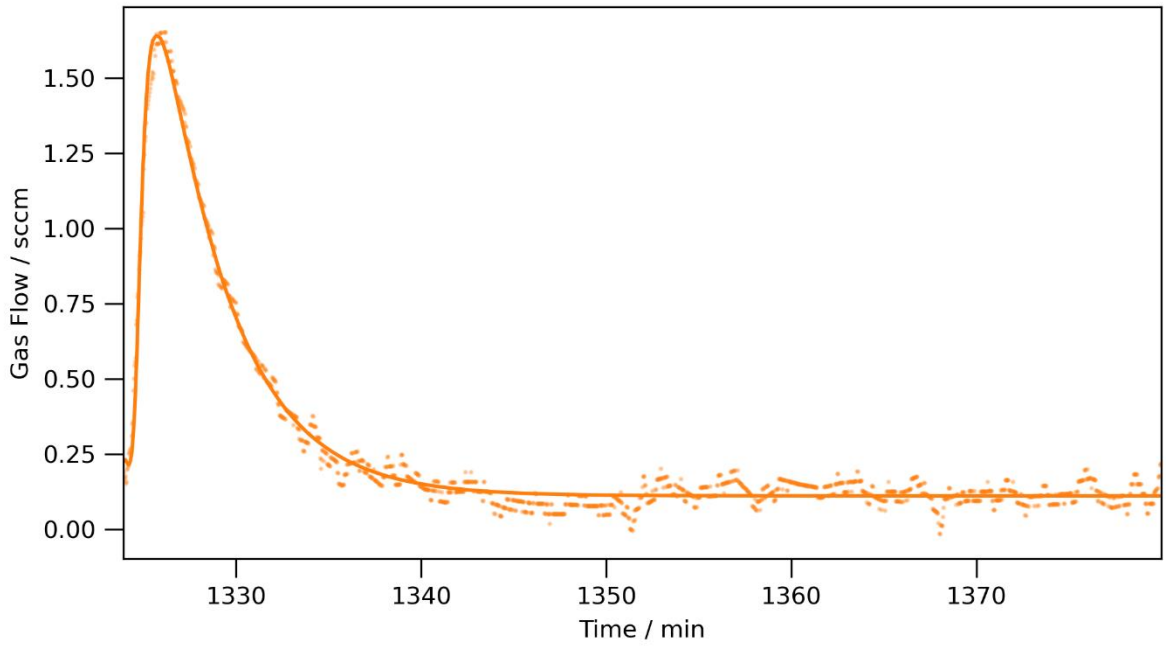

Figure S 12: Single exponential fit to the N_2 release at 520°C for the $LiNH_2$-Cr experiment.

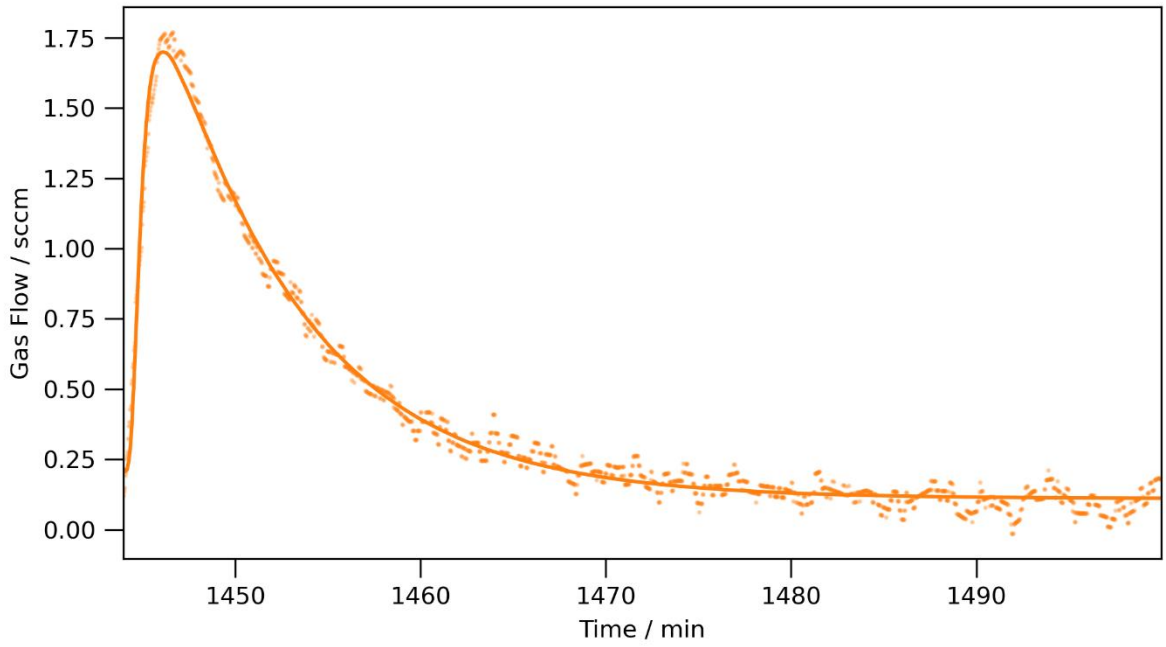

Figure S 13: Single exponential fit to the N_2 release at 540°C for the $LiNH_2$-Cr experiment.

$LiNH_2$-Mn experiment

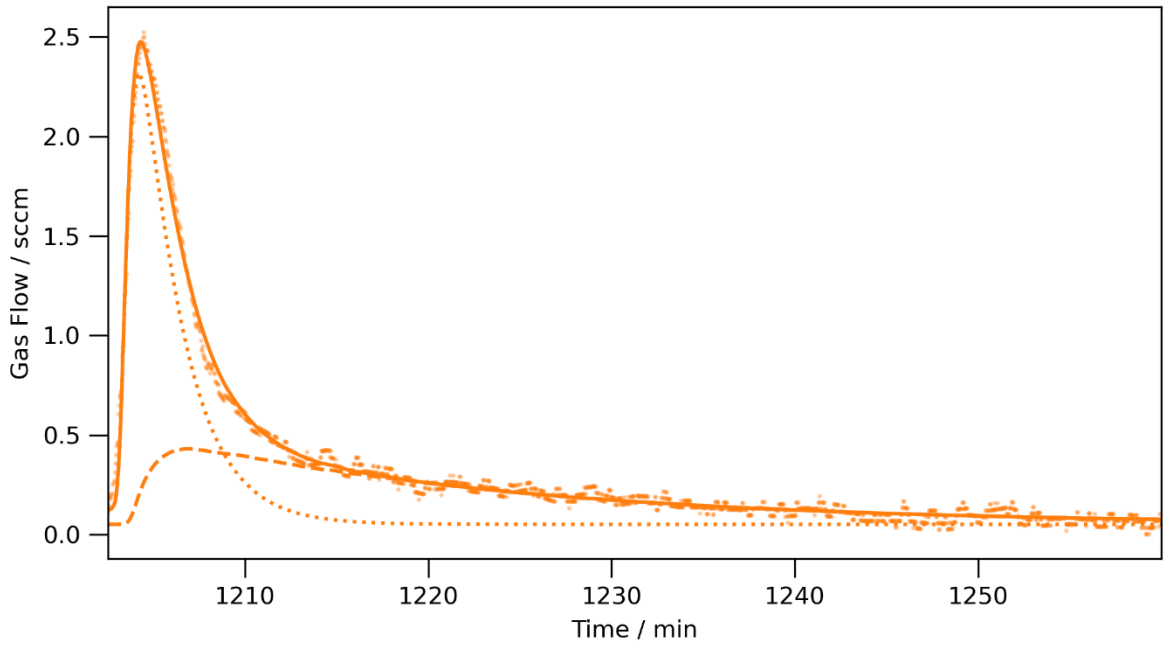

Figure S 14: Double exponential fit to the N_2 release at 500°C for the $LiNH_2$-Mn experiment. Dotted and dashed lines correspond with each component exponential curve, while the solid line is the summed fit.

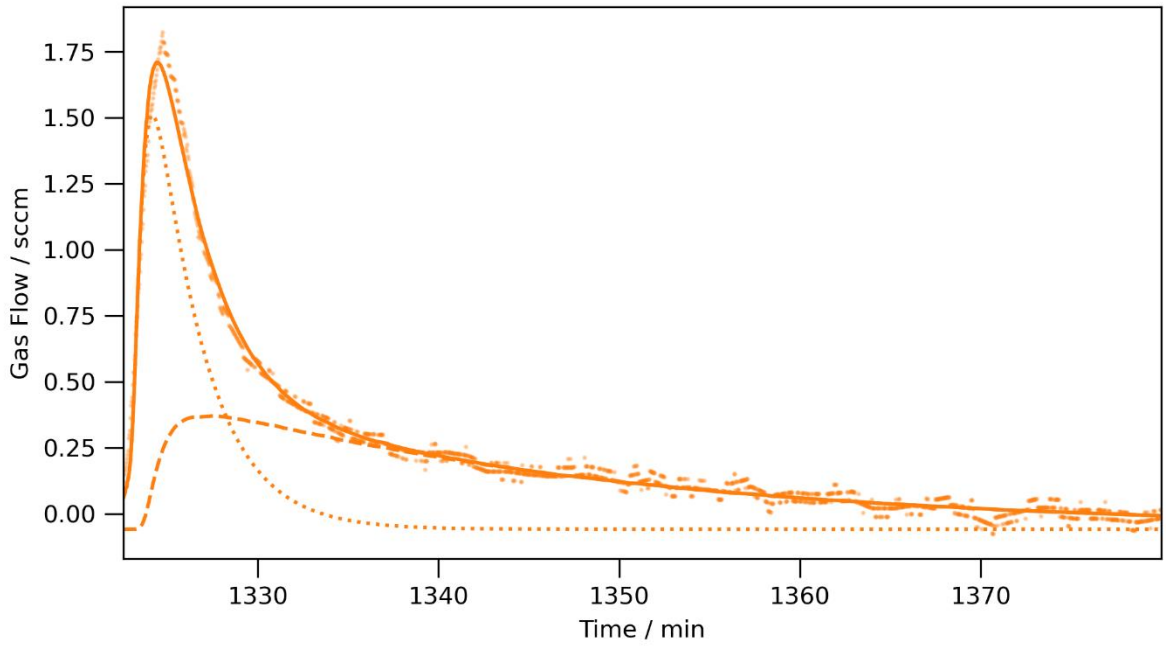

Figure S 15: Double exponential fit to the N_2 release at 520°C for the $LiNH_2$-Mn experiment. Dotted and dashed lines correspond with each component exponential curve, while the solid line is the summed fit.

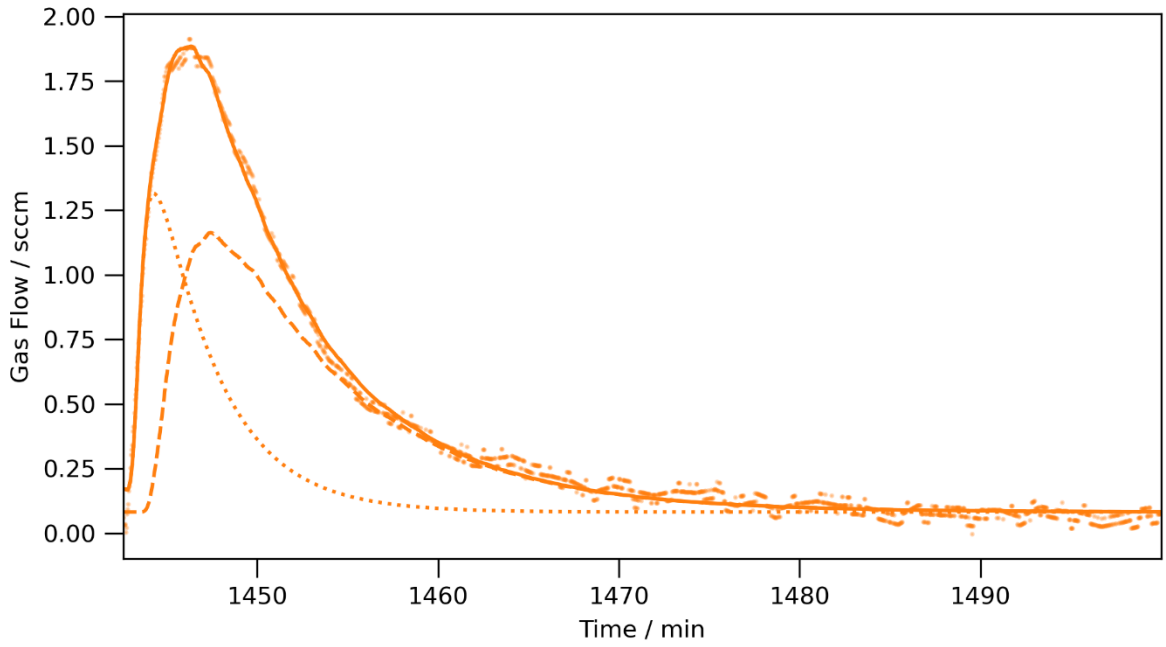

Figure S 16: Double exponential fit to the N_2 release at 540°C for the $LiNH_2$-Mn experiment. Dotted and dashed lines correspond with each component exponential curve, while the solid line is the summed fit.

$LiNH_2$-Fe experiment

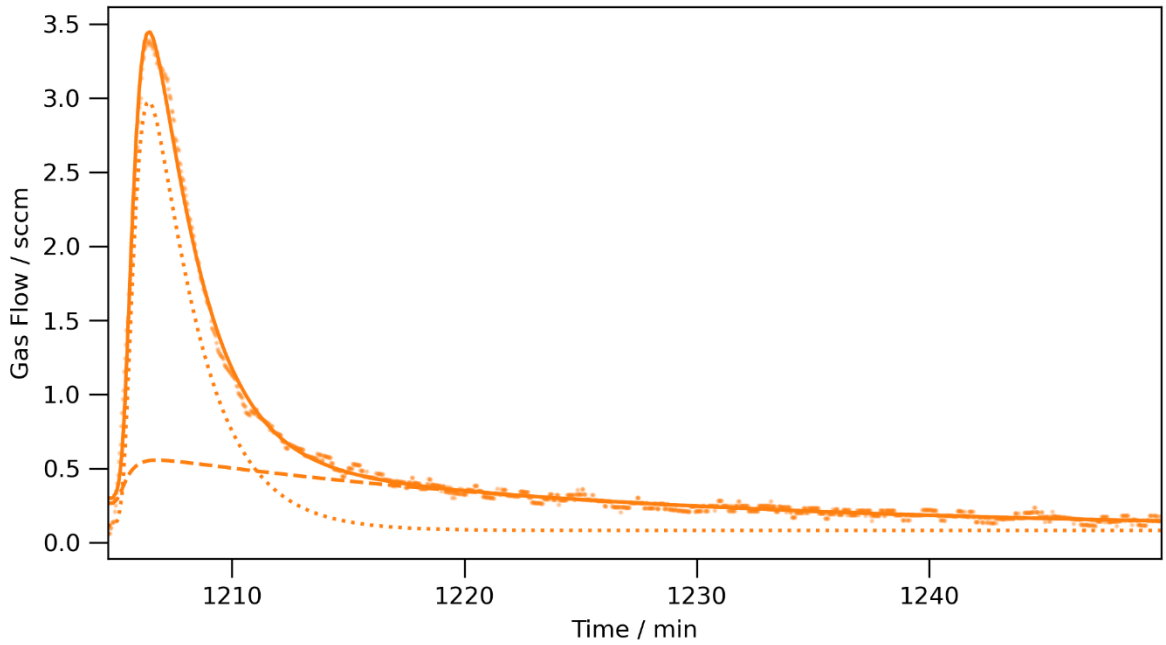

Figure S 17: Double exponential fit to the N_2 release at 500°C for the $LiNH_2$-Fe experiment. Dotted and dashed lines correspond with each component exponential curve, while the solid line is the summed fit.

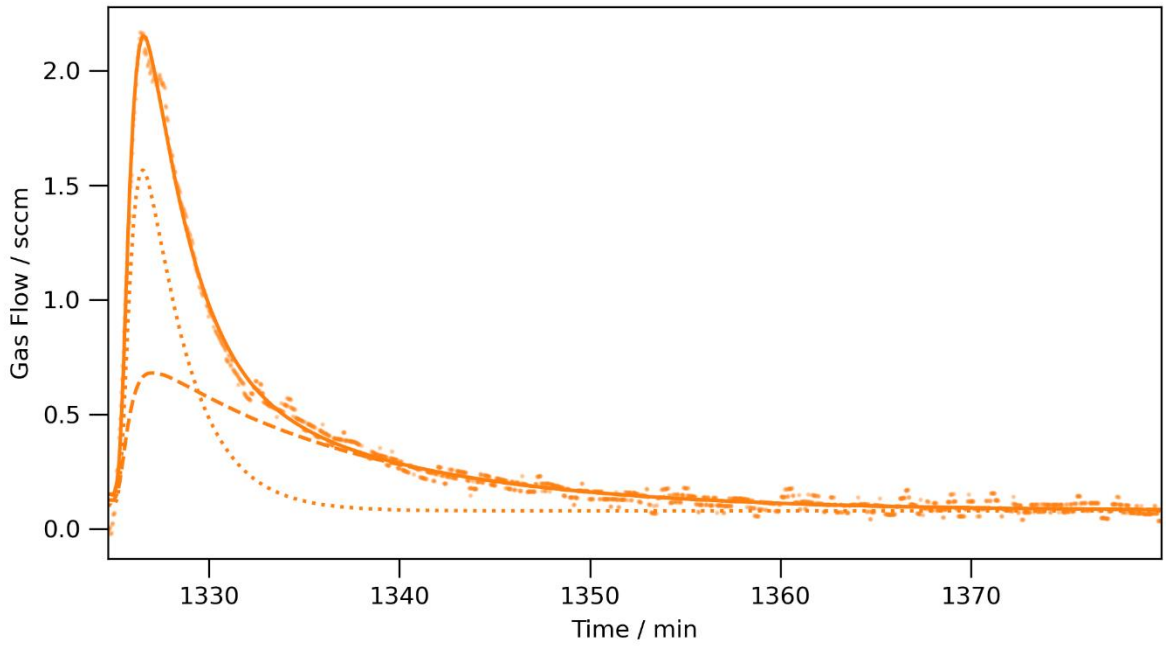

Figure S 18: Double exponential fit to the N_2 release at 520°C for the $LiNH_2$-Fe experiment. Dotted and dashed lines correspond with each component exponential curve, while the solid line is the summed fit.

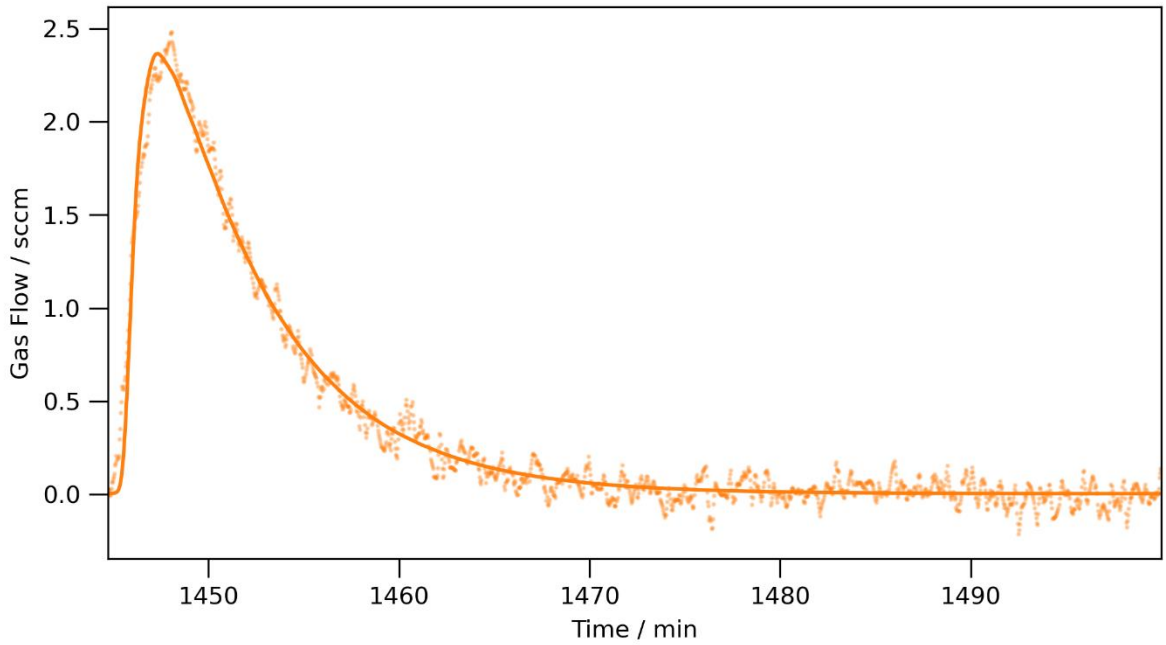

Figure S 19: Single exponential fit to the N_2 release at 540°C for the $LiNH_2$-Cr experiment. Dotted and dashed lines correspond with each component exponential curve, while the solid line is the summed fit.

Table S 1: Time constants of exponential fits to the N_2 flow data of blank reactor, $LiNH_2$, and $LiNH_2$-TM ammonia decomposition experiments during the highest three temperature increments.

	Time constant for gas release per temperature rise / min					
	500°C		520°C		540°C	
Blank	2.53(2)	21.0(2)	-	-	4.67(4)	26.9(2)
$LiNH_2$	2.12(4)	7.5(3)	2.63(4)	13.8(9)	7.29(6)	-
$LiNH_2$-Cr	1.63(7)	6.19(16)	3.69(3)	-	7.50(5)	-
$LiNH_2$-Mn	2.17(3)	19.0(7)	2.67(5)	23.9(14)	3.33(3)	7.47(6)
$LiNH_2$-Fe	2.03(4)	21(3)	2.16(12)	10.9(5)	5.76(7)	-

TG-DTA of $LiNH_2$-TM (TM = Cr, Fe, Mn) systems

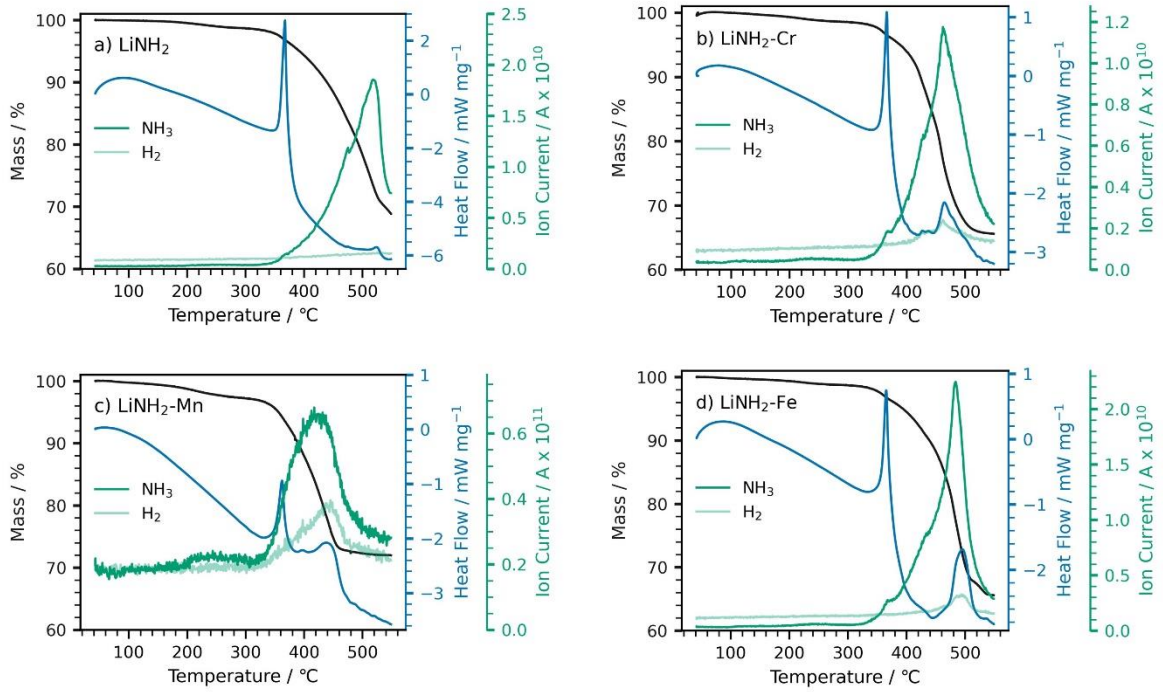

Figure S 20: Combined TG, DTA, and MS results from the gravimetric study of $LiNH_2$-TM systems under a 70 sccm N_2 flow. Shown are the gravimetric (black), heat flow (blue), and MS m/z=17 (NH_3) and m/z=2 (H_2) data.

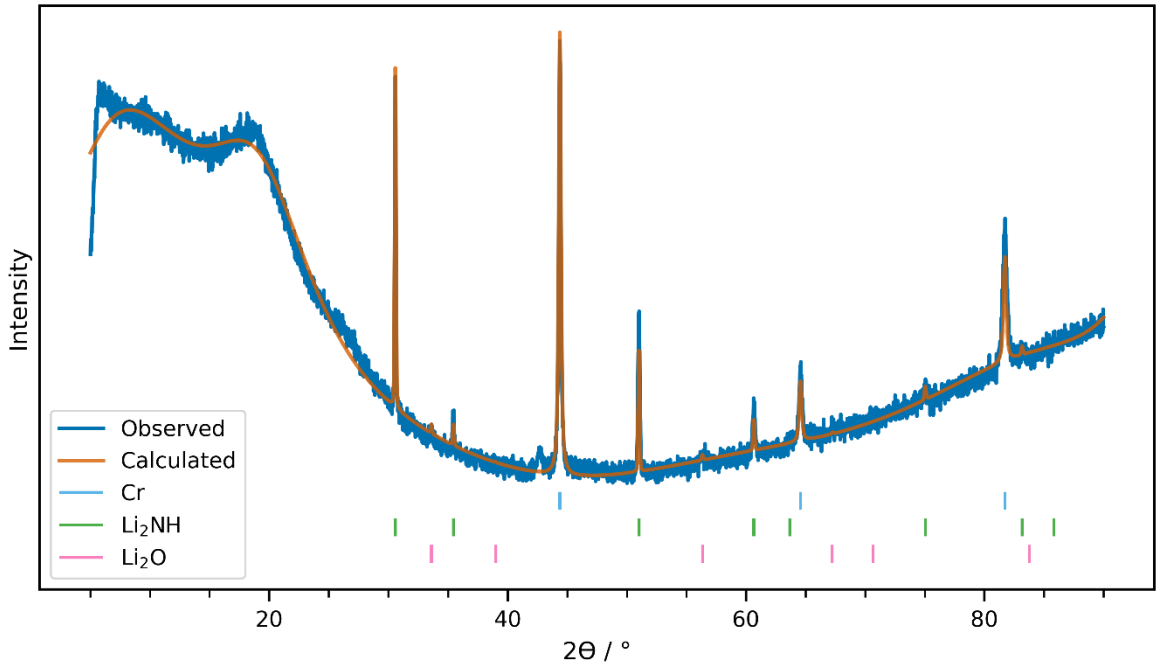

Figure S 21: X-ray powder diffraction pattern (Cu X-ray source) of the $LiNH_2$-Cr post-reaction material after heating under 70 sccm argon flow (5°C min^{-1} to 550°C). A similar experimental design but a greater mass of sample (0.2 g) was used to the simultaneous thermal analysis experiment. Shown are the observed data (blue), refined fit (orange) and tick positions of the included phases.

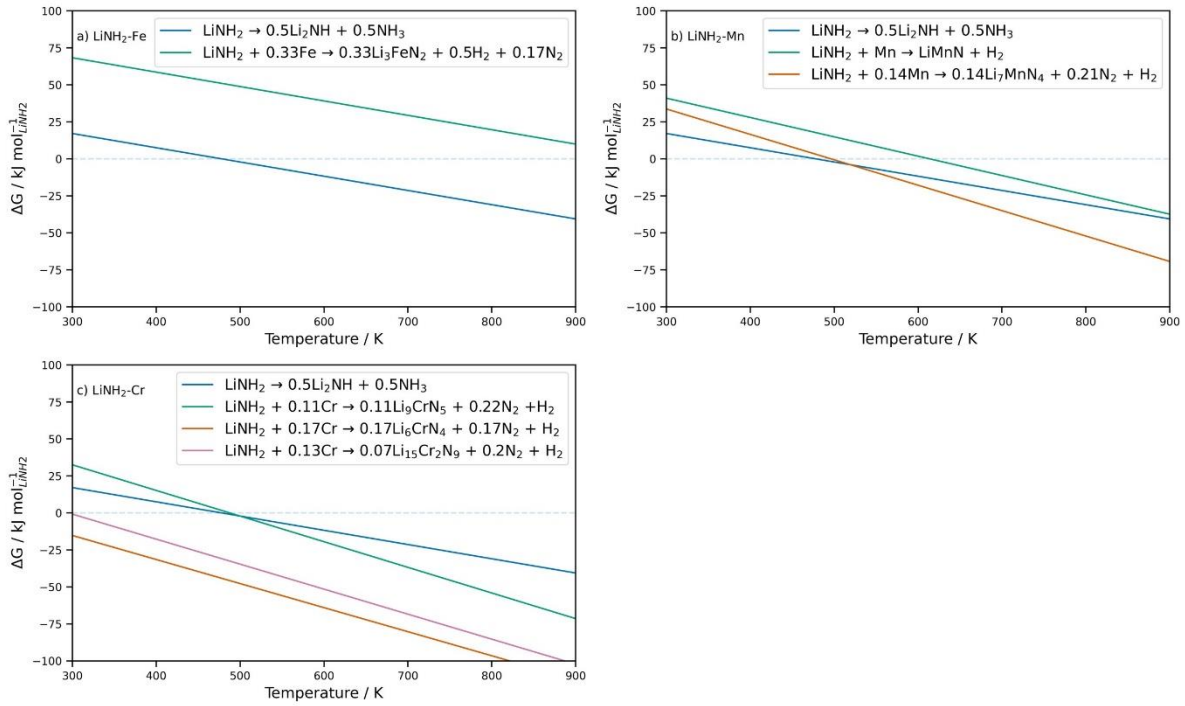

Figure S 22: Gibbs free energy of lithium ternary nitride formation reactions. Reaction enthalpies have been calculated from the literature values for $LiNH_2$ [1] and ternary nitrides [2–6]. The entropic contributions of solid crystalline reactants and products are ignored.

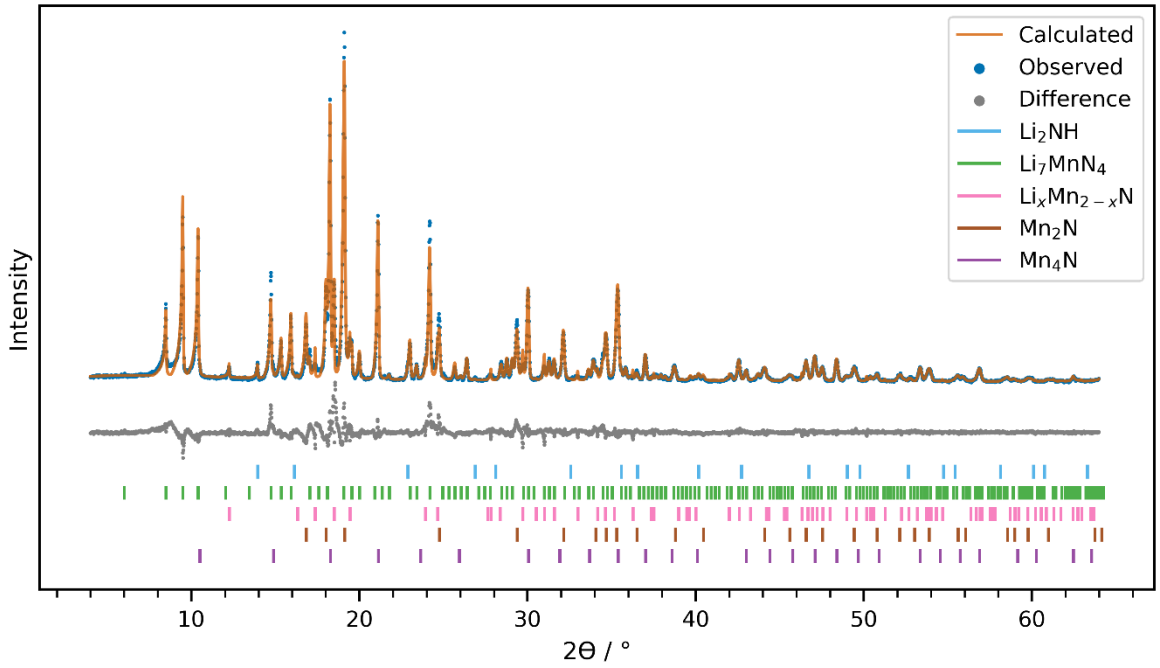

Figure S 23: X-ray powder diffraction pattern (Mo X-ray source) of the $LiNH_2$-Mn material after the simultaneous thermal analysis experiment. Shown are the observed data (blue), refined fit (orange), difference between them (grey), and tick positions of the included phases.

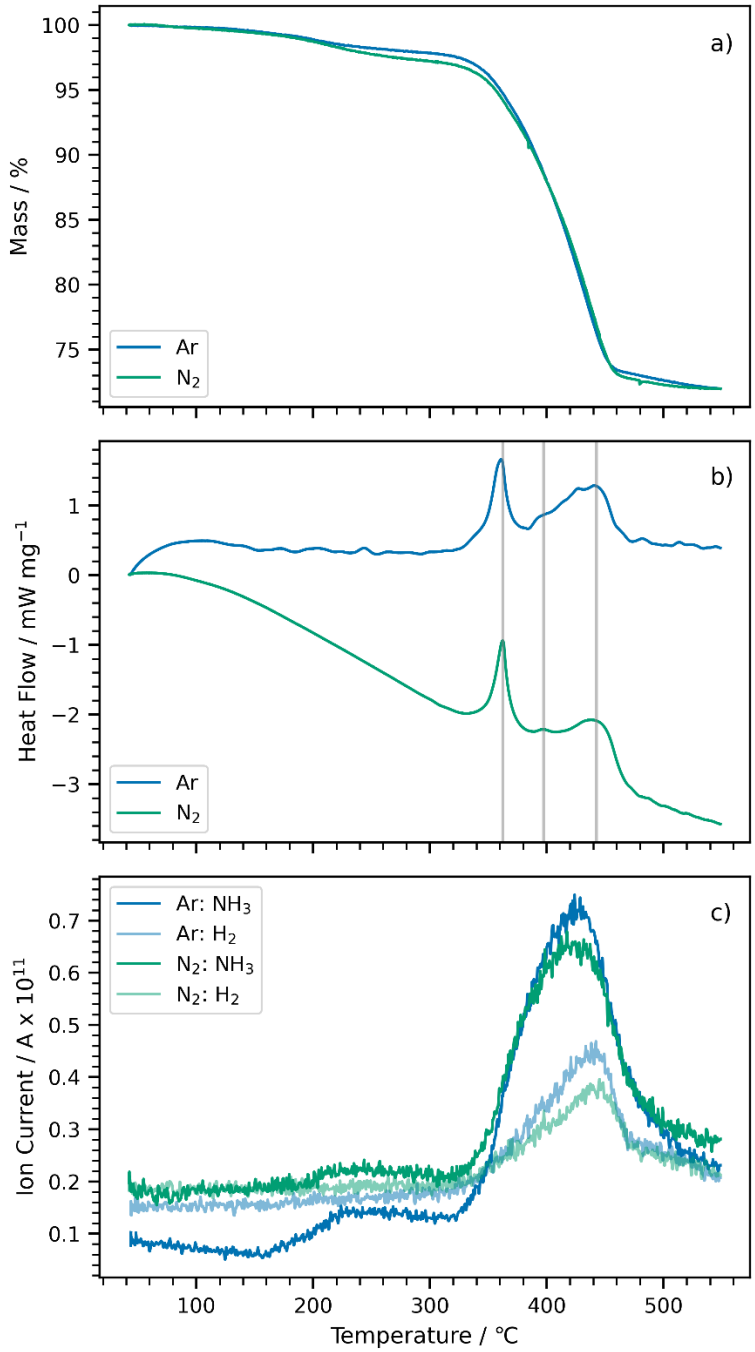

Figure S 24: Comparison between $LiNH_2$-Mn gravimetric study using either 70 sccm N_2 (green) or Ar (blue) flow. a) Shows the TG, b) the DTA, and c) m/z=17 (dark, NH_3) and m/z=2 (light, H_2) exhaust mass spectrometry data.

XRD patterns of post-catalytic transition metal-only materials

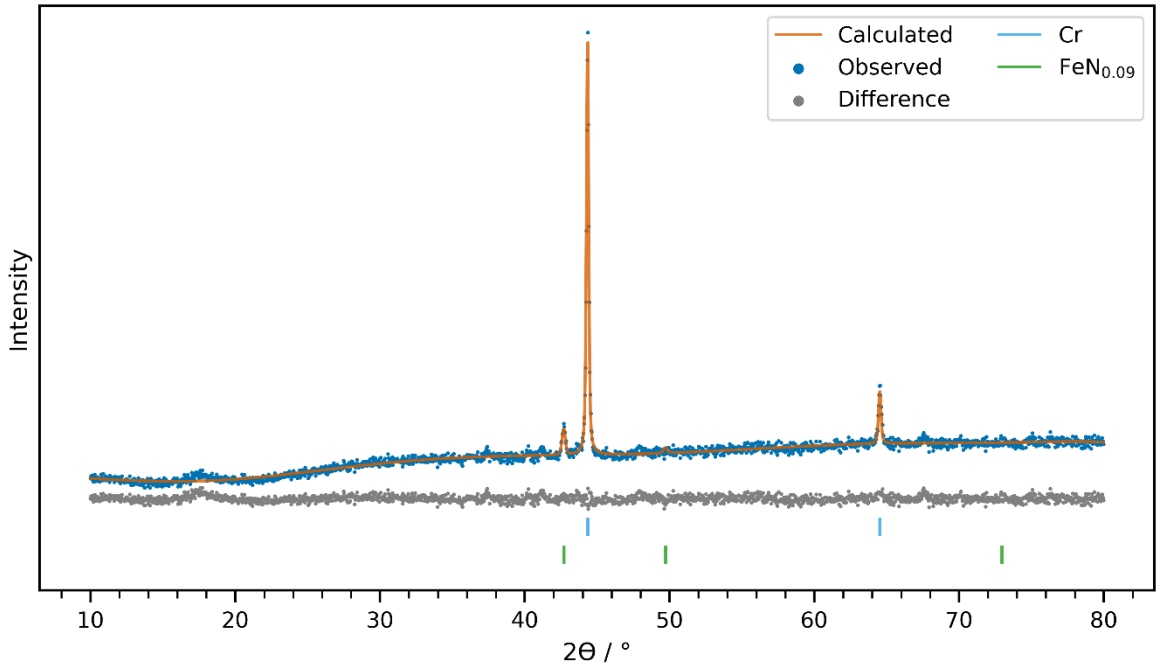

Figure S 25: X-ray powder diffraction pattern (Cu X-ray source) of the Cr-only sample after the catalytic experiment. Shown are the observed data (blue), refined fit (orange), difference between them (grey), and tick positions of the included phases.

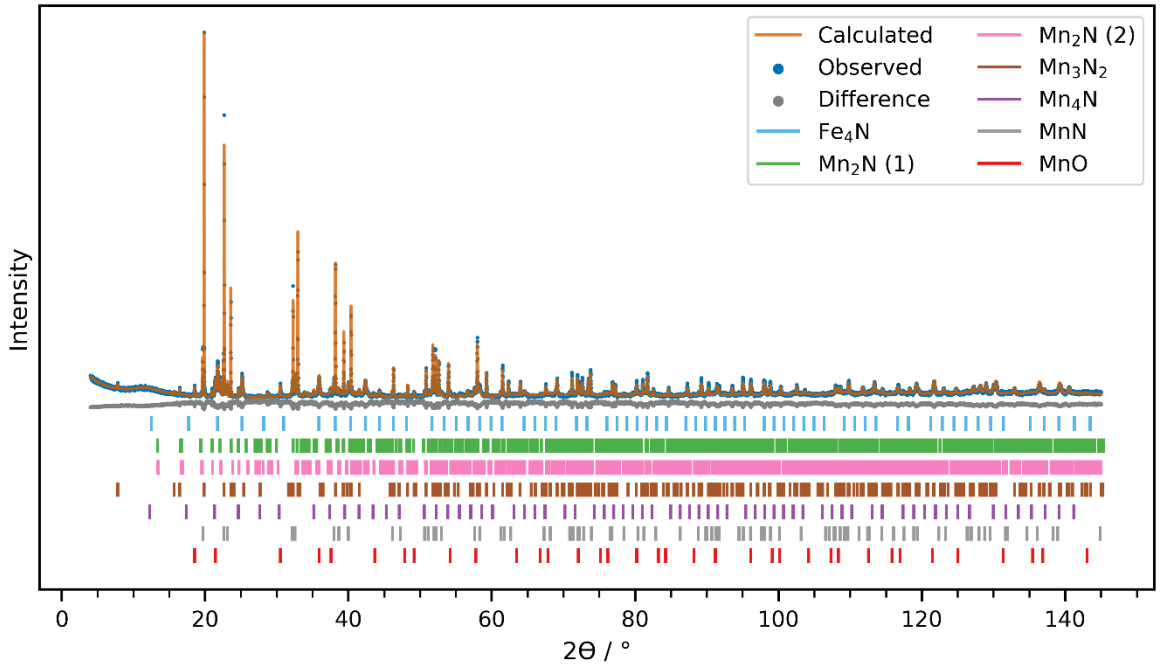

Figure S 26: X-ray powder diffraction pattern (synchrotron X-ray source, λ = 0.8268226 Å) of the Mn-only sample after the catalytic experiment. Shown are the observed data (blue), refined fit (orange), difference between them (grey), and tick positions of the included phases.

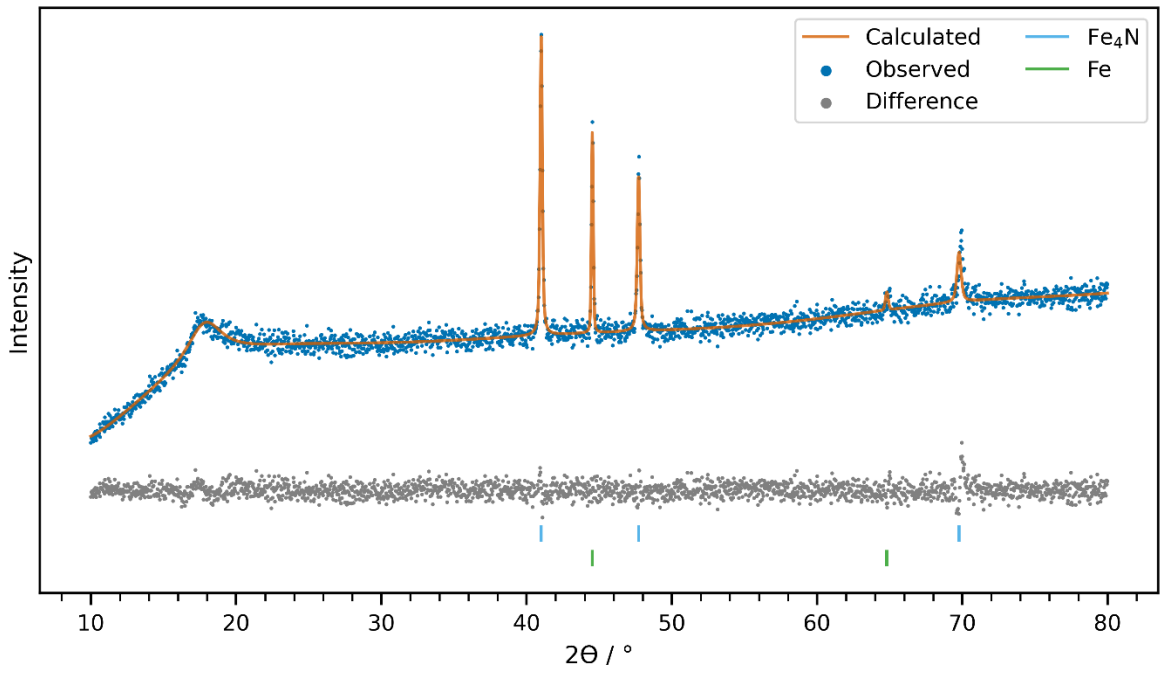

Figure S 27: X-ray powder diffraction pattern (Cu X-ray source) of the Fe-only sample after the catalytic experiment. Shown are the observed data (blue), refined fit (orange), difference between them (grey), and tick positions of the included phases.

References

1. Reed JJ, National Institute of Standards and Technology. The NBS Tables of Chemical Thermodynamic Properties: Selected Values for Inorganic and C1 and C2 Organic Substances in SI Units. 1989. DOI: 10.18434/M32124.

2. Jain A, Ong SP, Hautier G, Chen W, Richards WD, Dacek S, et al. Materials Project. 2013. https://materialsproject.org/. (accessed 29 Oct 2021).

3. Herbst JF, Hector LG. Exploration of the formation of XLi 3N 2 compounds (X = Sc-Zn) by means of density functional theory. Phys Rev B - Condens Matter Mater Phys. 2012, 85(19): 195137. DOI: 10.1103/PhysRevB.85.195137.

4. Sun W, Bartel CJ, Arca E, Bauers SR, Matthews B, Orvañanos B, et al. A map of the inorganic ternary metal nitrides. Nat Mater. 2019, 18(7): 732–9. DOI: 10.1038/s41563-019-0396-2.

5. Popovich A, Novikov P, Wang Q, Pushnitsa K, Aleksandrov D. Synthesis method and thermodynamic characteristics of anode material Li3FeN2 for application in lithium-ion batteries. Materials (Basel). 2021, 14(24): 7562. DOI: 10.3390/ma14247562.

6. Tessier F, Ranade MR, Navrotsky A, Niewa R, DiSalvo FJ, Leineweber A, et al. Thermodynamics of formation of binary and ternary nitrides in the system Ce/Mn/N. Zeitschrift fur Anorg und Allg Chemie. 2001, 627(2): 194–200. DOI: 10.1002/1521-3749(200102)627:2<194::AID-ZAAC194>3.0.CO;2-0.